Article

Diagenesis and Reservoir Evolution Model of the Ediacaran Dengying Formation in the Sichuan Basin: Evidence from Laser Ablation U-Pb Dating and In Situ Isotope Analysis

Zhanfeng Qiao [1,2,*], Jianhua Dong [3,4,*], Zhou Yu [1,2], Wenzheng Li [1,2], Xiaofang Wang [1,2], Lei Jiang [5,6] and Hairuo Qing [7]

1   PetroChina Hangzhou Research Institute of Geology, Hangzhou 310023, China
2   CNPC Key Laboratory of Carbonate Reservoir, Hangzhou 310023, China
3   State Key Laboratory of Petroleum Resource and Prospecting, China University of Petroleum (Beijing), Beijing 102249, China
4   College of Geosciences, China University of Petroleum (Beijing), Beijing 102249, China
5   Key Laboratory of Cenozoic Geology and Environment, Institute of Geology and Geophysics, Chinese Academy of Sciences, Beijing 100029, China
6   Institutions of Earth Science, Chinese Academy of Sciences, Beijing 100029, China
7   Department of Geology, University of Regina, Regina, SK S4S 0A2, Canada
*   Correspondence: qiaozf_hz@petrochina.com.cn (Z.Q.); dongjh_1222@163.com (J.D.)

Abstract: The microbial dolomite of the Ediacaran Dengying Fm., Sichuan Basin, SW China is endowed with abundant oil and gas resources. A complex diagenetic history greatly complicates the development of such microbial dolomite reservoirs, and has severely restrained hydrocarbon exploration. This study focused on key field profiles in Eastern Sichuan and aimed to decipher the origin and evolution of dolomites, using novel techniques, including elemental mapping, laser ablation U-Pb dating as well as carbon, oxygen, and strontium isotope analyses. Additionally, we compared the diagenesis and reservoir development model for the Dengying microbial dolomites of the Central Sichuan to other areas, with the aim to provide practical guidance for oil and gas exploration across the entire Sichuan Basin. Our results have shown that the Ediacaran microbial dolomite in Eastern Sichuan experienced four stages of diagenetic modification–specifically: (1) syn-sedimentary dolomitization; (2) penecontemporaneous cementation of fibrous dolomite cement; (3) bladed dolomite and brown-dark very fine crystalline dolomite cementation during the Ordovician; and (4) fine crystalline dolomite and medium-coarse crystalline dolomite cementation during the Silurian-Devonian. Petrology and geochemistry data imply that each diagenetic phase of dolomitization was mainly sourced from marine-dominated fluids. The influence of tectonically related fluids was rarely noted. Significantly, U-Pb ages of these dolomites reveal that the history of dolomite infill to pores within the Eastern Sichuan Basin clearly post-dated that in the Central Sichuan region, resulting in high porosities (6%–11%) that favored hydrocarbon accumulation. This study suggests that the platform margin at the eastern edge of the Xuanhan-Kaijiang paleo-uplift is favorable as the next key exploration target for microbial dolomites in the Sichuan Basin.

Keywords: dengying formation; microbial dolomite; elemental mapping; laser ablation U-Pb dating; in situ isotope; diagenetic pore evolution; Sichuan Basin

1. Introduction

Microbial carbonate rocks commonly contain abundant oil and gas resources [1]. Examples include the Little Cedar Creek oilfield in the USA [2,3], the pre-salt oilfields in the Santos Basin, Brazil [4], those of Aman in the Middle East [5,6], and the Tangiz oilfield in Caspian Basin, Kazakhstan [7]. Large gas reservoirs (Weiyuan and Gaoshiti) have similarly been discovered in microbialite of the Ediacaran Dengying Formation in the

Sichuan Basin in China, and have considerable potential for hydrocarbon exploration in the next decades [8,9].

The Denying Formation from the Sichuan Basin is dominated by microbial dolomite [10,11]. Previous researchers of these microbial dolomites have predominantly focused on dolomitization models that include sabkha, seepage reflux, and burial dolomitization [12]. Additionally, there have been multiple mechanisms proposed for the genesis of Sininian microbial dolomite reservoirs in Central Sichuan Basin, including the karstification [13,14], (pene)contemporaneous microbial framework pores [10,15,16], and hydrothermal dissolution [17,18]. However, the coupling relationships between diagenesis and reservoir formation are not yet clear [19]. In particular, for microbial carbonate rocks which were subjected to a prolonged or complex diagenesis, the situation is more complicated. Therefore, it is challenging to determine whether or not effective pores were present prior to hydrocarbon emplacement. Furthermore, the different diagenetic models for microbial dolomites throughout the Sichuan Basin also lead to difficulties in effective reservoir prediction. Hence, it is essential to study the diagenetic processes and reservoir-forming models of microbial dolomites in different locations, to better address the needs of hydrocarbon exploration in this region.

Recently, great achievements have been made in in situ geochemical testing technology and laser ablation U-Pb dating techniques, as applied to diagenetic studies [20–36]. The laser mapping technique has been applied to oolitic limestone [20], abiogenic laminated carbonate rocks [21], microbial dolomite cement [25], burial dolomite [30], and hydrothermal dolomite [31]. Meanwhile, laser ablation U-Pb dating has been applied to the investigation of microbial dolomite cement [24,25], hydrothermal dolomite [27,31], biodetritus [33], calcite cement [32,34], hydrothermal calcite vein [35], and limestone alteration [36]. These techniques make it possible to better decipher the diagenetic histories and reservoir-forming models of carbonate rocks.

This study focused on the Ediacaran Dengying Formation microbial dolomite in the Hanfengya and Bajiaoxi profiles in Eastern Sichuan. By integrating diagenetic sequence study, with several novel technical approaches, including trace and rare earth elements (REEs) elemental mapping, laser ablation carbon, oxygen, and strontium isotope compositions, and laser ablation U-Pb dating, the diagenetic and reservoir-forming processes of these microbial dolomites were precisely constrained. We further compared the differentiated diagenetic mechanisms and their reservoir development patterns of these Ediacaran microbial dolomites in typical areas from the Sichuan Basin, providing guidance for future oil and gas exploration across this region of China.

2. Geological Setting

The Sichuan Basin, located in Southwestern China (Figure 1a), is a basin with a complex tectonic and sedimentary history, relating to evolution of the upper to middle Yangtze Plate [37]. During the Late Mesoproterozoic, under the influence of the breakup of the Rodinia supercontinent, the Yangtze Plate initiated separation from the Rodinia supercontinent, while the synsedimentary fault activity resulted in the formation of the Deyang-Anyue and Chengkou-Exi rifts within the Mid-Upper Yangtze Craton [38] (Figure 1b).
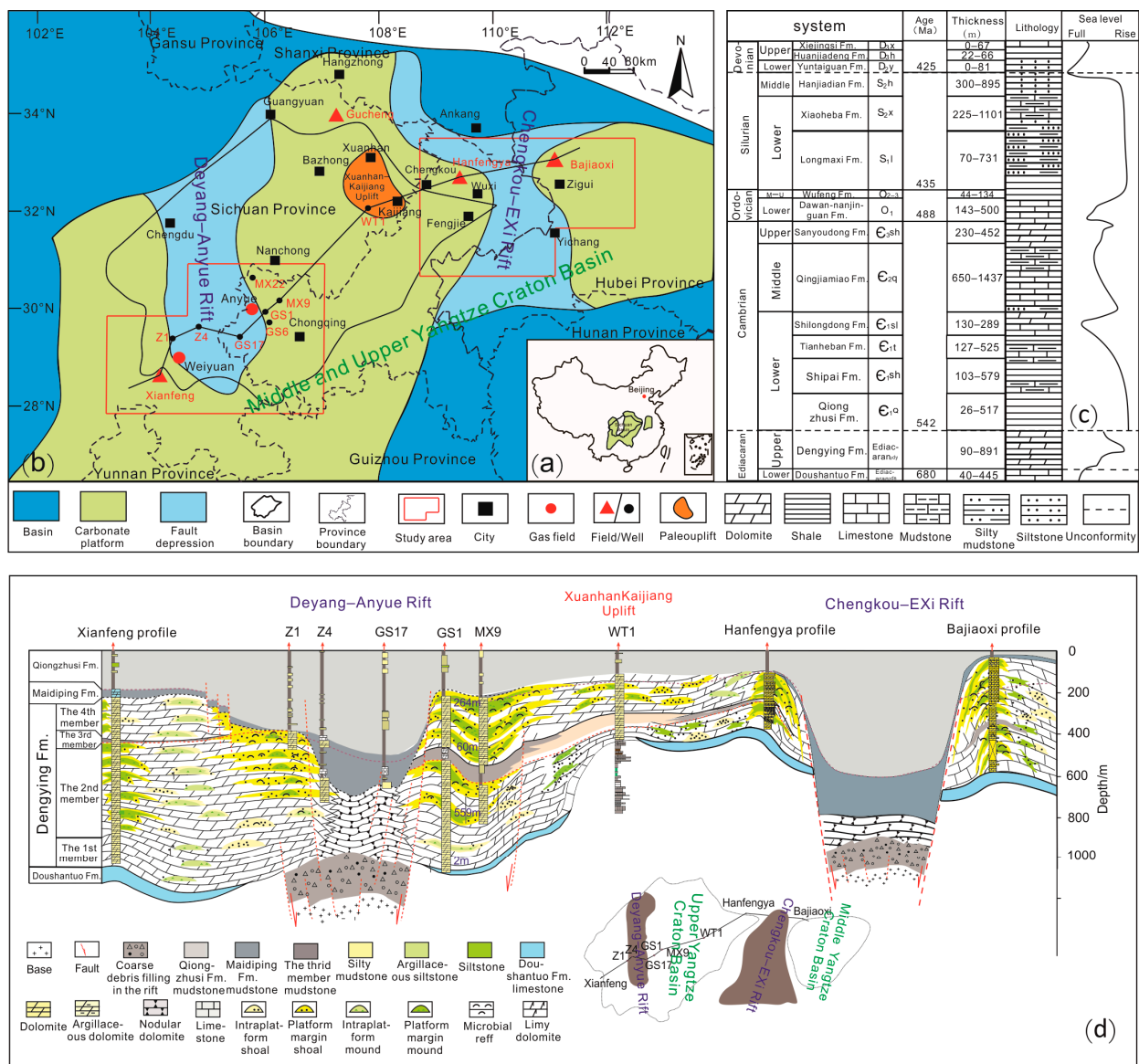
Figure 1. Geological Setting. (**a**) Location of the Sichuan Basin in Southwestern China; (**b**) paleogeographic framework of the Late Ediacaran Eastern Sichuan (modified from [38]); (**c**) the stratigraphic column of the Ediacaran-Devonian in Eastern Sichuan (modified from [39]); (**d**) stratigraphic cross section of the Dengying Formation in the Mid-Upper Yangtze Craton, flattened by the top of Qiongzhusi Formation (modified from [38]).

The deposition of the Ediacaran Dengying Formation, within the Sichuan Basin, was dominated by a large carbonate platform, surrounded by deep marine deposits, and influenced by the Deyang-Anyue- and Chengkou-Exi rifts of the Central and Eastern Sichuan Basin, respectively (Figure 1b). Paleomagnetic data indicate that the Sichuan Basin was equatorially located during the Ediacaran Period [40]. Along the platform margin and margins of rifts, large amounts of microbial reefs occur (Figure 1b) [41]. The study area lies in the eastern part of the Sichuan Basin (Eastern Sichuan; Figure 1b), which is at the margin of the Mid-Upper Yangtze Craton.

The Dengying Formation sits atop of the Doushantuo Formation and is divided into four Members in the Sichuan Basin (Figure 1c). It is capped by the Maidiping Formation or Qiongzhusi Formation with unconformity boundaries, in which Maidiping Formation only occurs within the rifts. In the Sichuan Basin region, four members of Dengying Formation have similar lithologies but variable thicknesses (Figure 1d). The 1st Member

(Z$_2$dn1) is composed of dark gray, laminated, finely crystalline dolomite interbedded with light gray laminated medium crystalline dolomite; the 2nd Member (Z$_2$dn2) consists of laminated microbial dolomite with a typical birds-eye structure and thickly bedded microbial dolomite that features botryoidal structures; the 3rd Member (Z$_2$dn3) includes basal siliciclastic rocks and crystalline dolomite; the 4th Member (Z$_2$dn4) is characterized by the intraclastic bindstone to grainstone. The 3rd and 4th Members are not developed within the rifts.

Multiple tectonic movements played important roles in the deposition and subsequent burial process of the Dengying Formation, including the Tongwan, Caledonian, Hecynian, Indocinian, Yanshanian, and Himalaya tectonic activities. First, under the influence of the two episodes of the Tongwan movement, the 2nd and 4th Members experienced to different extents, dissolution or karstification, and were each capped by unconformities [41–43]. Moreover, these, in combination with the influence of subsidence, lead to considerable differentiation in the thickness of the Dengying Formation over the Sichuan Basin. During the Cambrian, the Dengying Formation kept subsiding steadily, but the subsidence was much greater in the Eastern Sichuan Basin than for the Central Sichuan Basin (Figure 2). The Caledonian movement exerted important effects on the Sichuan Basin. The local-named Duyun movement occurred during the Ordovician and caused uplift of Guizhou Province as well as Eastern Sichuan Basin. The entire Sichuan Basin experienced significant uplift in response to the Early Hercynian movement and rapid subsidence due to the Late Hercynian movement. Finally, the Yanshanian movement uplifted and exposed the Dengying Formation in the Eastern Basin, while in Central Sichuan Basin, the Dengying Formation was kept at or near subsurface.
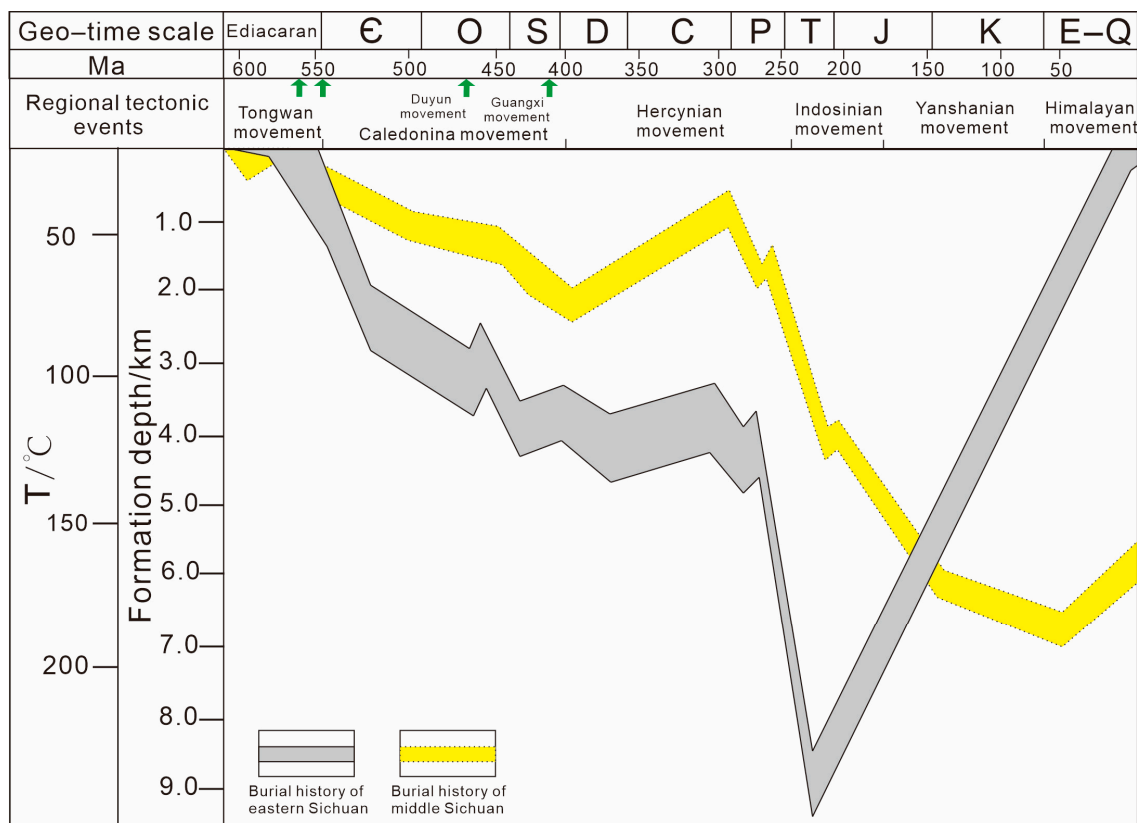
Figure 2. Typical burial history of the Ediacaran Dengying Formation, Sichuan Basin (Eastern Sichuan, modified from [44]; and for Central Sichuan is modified from [45]).

3. Material and Methods

3.1. Field Survey

Field surveys were carefully performed on the Hanfengya and Bajiaoxi profiles in Eastern Sichuan Basin, including stratigraphy, lithology, sedimentary structure, diagenetic features, pore types, etc. Since the Dengying Formation consists of different types of microbial dolomite, dolograinstone, and crystalline dolomite, the descriptions presented below adopt the classifications of microbial carbonate by Riding [46], rock texture by Dunham [47], dolomite crystal by Gregg and Sibley [48] and Tucker and Wright [49], and pore types by Choquette and Pray [50] and Lønøy [51]. The data and results of the Central Sichuan Basin [24] were cited for comparison.

3.2. Sample Selection

Based on the careful field surveys of the Hanfengya and Bajiaoxi profiles, 14 samples were collected from the 2nd and 4th Members of the Dengying Formation, which covered main rock textures and diagenetic products of reservoir sections. Since no reservoir occurs in either of the 1st and 3rd Members, little attention was paid to these in this study. The sampling positions are presented in Figure 3. The selected samples have well-developed pores and/or vugs and fillings, which allow studying of the diagenetic history of the Dengying Formation. Slabs and thin sections of 14 samples were made to examine their petrological features and to build a diagenetic sequence with the assistance of cathodoluminescence. Based on the built diagenetic sequence, two samples that contain all phases of diagenetic products were further chosen to perform systemic geochemical tests, including laser ablation U-Pb dating, laser ablation C, O, and Sr isotope compositions, and elemental mapping of trace elements and rare earth element (REEs) within these samples.
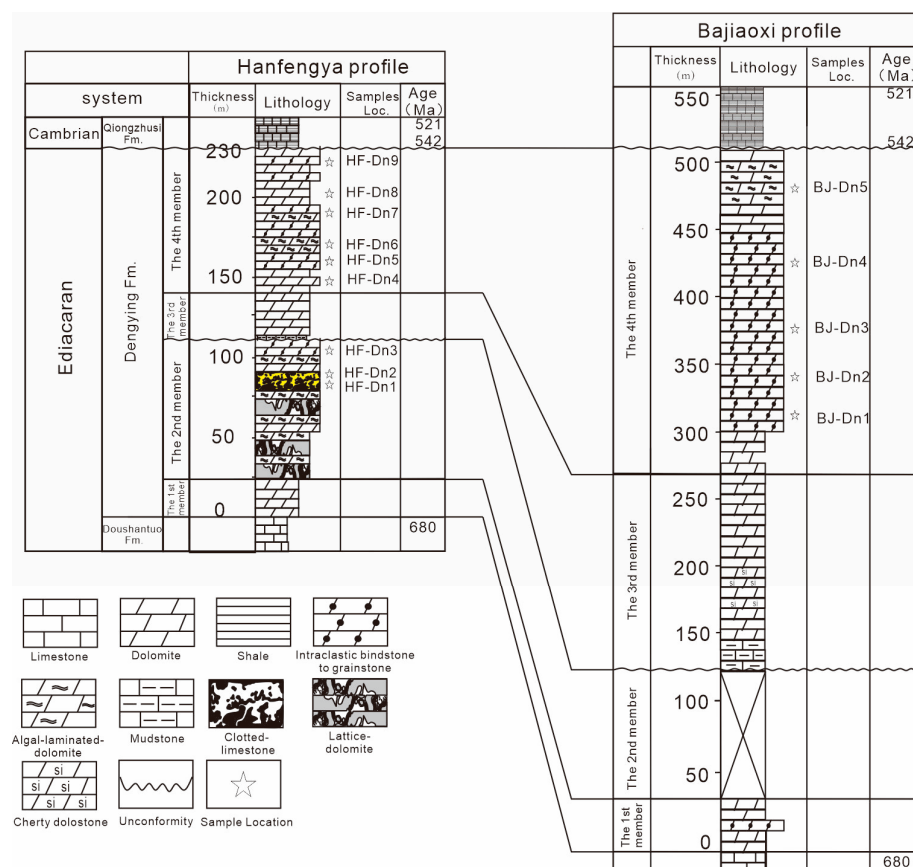

Figure 3. Cross section showing lithology and stratigraphic distribution of algal dolomite in the platform margin microbialite reef facies.

3.3. Experimental Analysis

For the analyzed samples, two groups of thin sections are prepared. One, with a thickness of 100 μm, was used for the cathodoluminescence (CL) microscopy, elemental mapping of trace elements and REEs, laser ablation U-Pb dating, and laser ablation strontium isotope analysis, and the other, with a thickness of 60 μm, was used for laser carbon and oxygen isotope analysis, respectively.

(1) CL examination was initially performed to distinguish different phases of diagenetic products. The instruments used were a polarizing microscope (DM2500P, Leica, Germany) and CL spectroscope (CL8200MK5, CITL, UK).

(2) Elemental mapping of trace elements and REEs was performed with a Thermo Fisher triple quadrupole inductively coupled plasma mass spectrometer (iCAP TQ, Thermo Fisher Scientific, Germany), combined with an Applied Spectroscopy laser denudation system (RESOlution LR S155, Applied Spectra Inc., USA). A square beam spot with a side length of 50 μm was used for denudation. The laser energy was 3 J/cm^2, the denudation frequency was 20 Hz, and the beam movement rate was 0.05 mm/s. First, 100 μm thin sections were polished with 2000, 3000, and 4000 mesh sandpaper to remove other mineral residues embedded on the sample surface. Second, the samples were repeatedly sonicated and cleaned with cleaning solution and Mill-Q water. Clean samples were then placed in a fume hood overnight or on a 50 °C hot plate to dry. Finally, the test area was selected for laser ablation. International standard samples NIST614, NIST612 and NIST610 were used for the test and calibration standard samples. Iolite software was used for data processing. The denudation interval of background, standard sample and sample was determined according to the laser log file. Semi-quantitative method was used for data processing. After checking the data results, the Sellspace Image method is used to scan the map. The detection limit is 1 ppb and the error on the analysis is 10%.

(3) Laser ablation U-Pb dating. ICap RQ inductively coupled plasma mass spectrometer (Thermo Fisher Scientific, Germany) and RESOlution laser denudation system (Applied Spectra Inc., Fremont, CA, USA) were used for U-Pb isotopic age determination of different samples by LASF-ICP-MS. Ahx-1 (age 209.8 ± 1.3 mA) from the Aksu area of the Tarim Basin and WC-1 (age 254 ± 6.4 Ma) from Calcite vein of Walnut Valley, USA were selected as standard samples for calibration. The beam spot diameter was 100 μm and the denudation frequency was 10 Hz. After loading into the sample target, the sample was cleaned to eliminate any common Pb contamination that might be present. The sampling method was single point laser denudation, and 70 points were sampled for each fabric. For data processing, Iolite 3.6 was used to process the original data online or offline, and the corresponding isotope ratios obtained were fitted to isochron age mapping on Isoplot 3.0 software.

(4) Laser ablation strontium isotope. The instruments used were a RESOlution LR 193 nm laser denudation system (Applied Spectra Inc., USA) and a Neptune Plus multi-receiver mass spectrometer (Thermo Fisher Scientific, Germany). The laser adopts 3 J/cm^2 energy density and a 285 μm beam spot to improve the sensitivity. The sample is denudated by line scanning with a denudation rate of 10 μm/s, helium flow rate of 350 ml/min and nitrogen flow rate of 1 ml/min. The carrier gas flow rate of the multi-receiver mass spectrometer was 1 L/min. To eliminate the interference of divalent rare earth element ions on strontium isotopes, the Faraday cup received signals at mass number positions of 83.5 and 85.5. Data acquisition adopts the process of first receiving the background signal for 30 s and then receiving the sample signal for 300 s. NIST614, NanoSr (0.70756 ± 0.00003 (2S) [52]) and XK1-9 (0.70890 ± 0.00002 (2S), dolomite, and internal laboratory standard samples were tested every five samples during the test process to monitor data quality. Iolite 3.65 was used for data processing [53]. The strontium isotopic composition of the sample was obtained by subtracting the background signal value and interference signal and correcting the instrument signal drift.

(5)　Laser ablation $\delta^{13}C$ and $\delta^{18}O$. Laser in situ carbon and oxygen isotope analysis was performed on a LA-IRMS instrument (Thermo Fisher Scientific, Germany). The laser equipment (Sichuan Xiwu Laser Technology co., LTD., Chengdu, China) was composed of Nd:YAG (Yttrium aluminum garnet) near-infrared laser, cooling system, microscopic imaging system, gas transmission, and the separation system. The Nd:YAG laser output a wavelength of 1064 nm near-infrared coherent laser beam. The beam spot size was less than 20 μm. A krypton lamp was used as the pump energy for the Nd:YAG laser, with an operating current of 7–20 A, and output energy of 7–40 W. The sample penetration depth for this method was 30–50 μm. In the process of laser denudation, helium was used as carrier gas, and CO_2 gas was produced by the interaction of laser and carbonate. After impurity gas separation and purification, pure CO_2 gas was obtained, which was tested and analyzed by isotope mass spectrometer. The laser beam spot and current of this analysis are 20 μm and 14–20 A, respectively, and the laser adopts continuous (CW) output mode. The standard sample used in the analysis data correction is the national standard GBW04405 and the laboratory standard sample 811. Data processing is completed by Thermo Fisher software ISODAT3.0.

All tests for this research were performed in the CNPC Key Laboratory of Carbonate Reservoir, Hangzhou, China.

4. Results

4.1. Petrological Characteristics

The reservoir rock of the Dengying Formation mainly consists of microbial dolostone and intraclastic bindstone to grainstone. The microbial dolostone were predominantly developed in the 2nd Member of the Dengying Formation, which consists of stromatolite dolostone, thrombolite dolostone, and laminated dolostone, whereas intraclastic bindstone to grainstone were mainly developed in the 4th Member of the Dengying Formation.

The stromatolite dolostone exhibits non-straight laminations (often wavy or dome-like and sometimes intermittent), displays considerable undulation (Figure 4a), and contains well-developed framework pores which are partially filled with crystalline dolomite. The laminated dolostone exhibits continuous laminations associated with abundant fenestral pores and siliceous layers (SB) (Figure 4b).

The thrombolite dolostone is characterized by an irregular microbial-like texture, interlayers of dark and light color mixed fabric (Figure 4c), and botryoidal structure (BS) [54] (Figure 4c) with non-fabric selective dissolution vugs that are filled by multiple stages of isopachous dolomite cements and crystalline dolomite (CD) (Figure 4d). The initial fibrous dolomite cement (FD-I) vertically encircles the boundaries of pores or grains (Figure 4d), showing dull-dark orange luminescence (Figure 4e). It consists of up to approximately 6% of the total vuggy porosity based on the estimation by point counting. It is followed by bladed dolomite cement (BD-II), which encircles the fibrous dolomite along the boundary and exhibits undulatory extinction and dark orange luminescence under CL (Figure 4e), occupying up to approximately 62% of the total vuggy porosity of large pores. Subsequently, brown-dark, very fine crystalline dolomite cement (BDD-III), which has no clear crystal forms (Figure 4d), was precipitated. It shows dark orange red luminescence (Figure 4e) and accounts up to approximately 9% of the total vuggy porosity. Fine crystalline dolomite cement (FCD-IV) precipitation was followed, which has clean bright crystals (mainly anhedral) (Figure 4d), shows the dark red luminescence under CL (Figure 4e), and occupies approximately up to 5% of the total vuggy porosity. Finally, medium-coarse crystalline dolomite (MCCD-V) cementation occurred, which is mainly subhedral-euhedral and shows bright orange red luminescence with the rim structure under CL examination (Figure 4e). It accounts for up to approximately 5% of the total vuggy porosity.
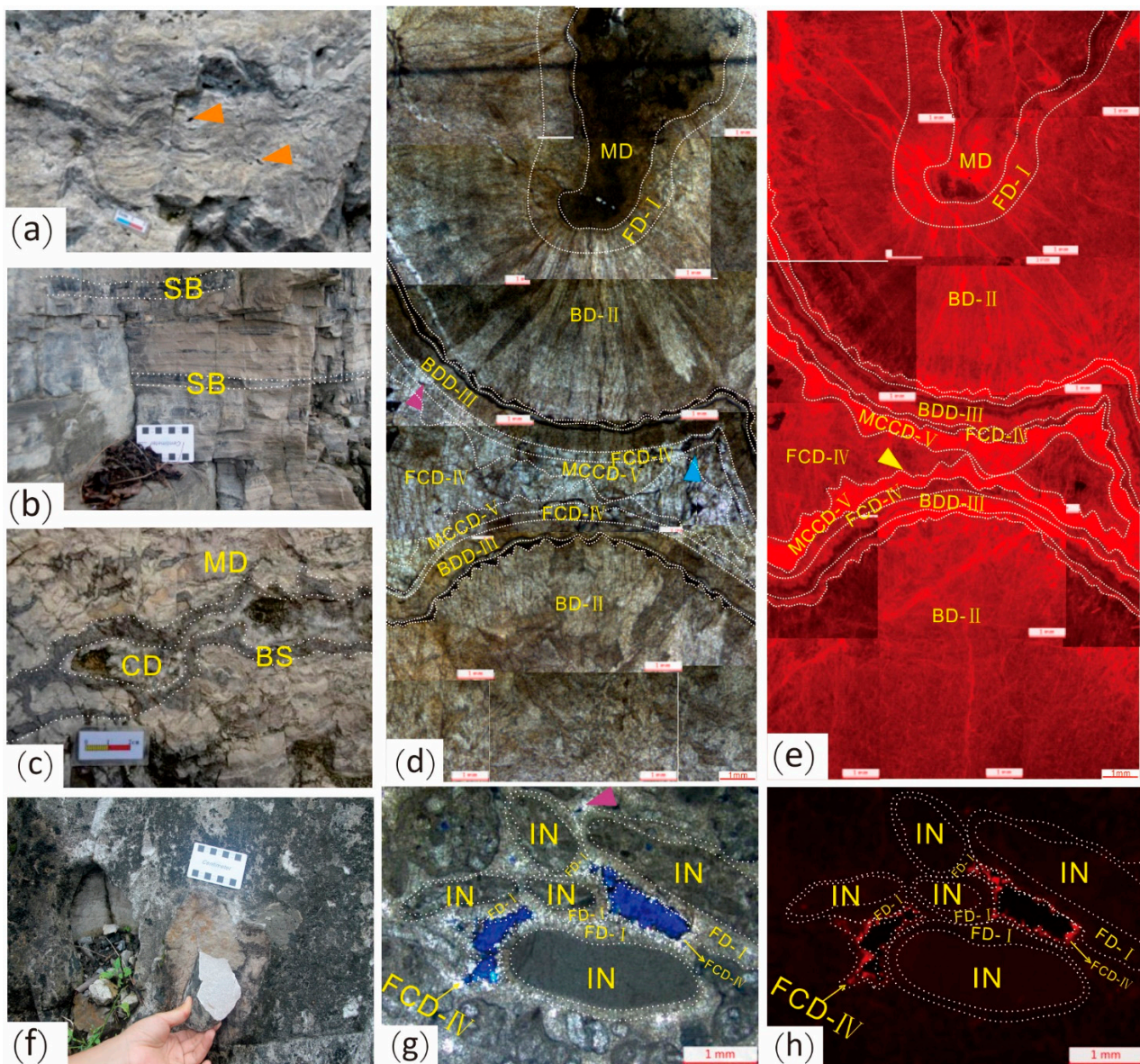
Figure 4. Petrographic characteristics of the microbial dolomite in the Dengying Formation, Eastern Sichuan. (**a**) Outcrop image, the 4th Member in the Bajiaoxi profile, stromatolite dolostone, with well-developed dissolution pores (by orange arrows); (**b**) Outcrop image, the 4th Member in the Bajiaoxi profile, laminated dolomite, with the development of siliceous layers (SB); (**c**) Outcrop image, the 2nd Member in the Hanfengya profile, showing sequence of thrombolite dolostone (MD), botryoidal structure (BS), and crystalline dolomite (CD), and their relationship to large vuggy porosity; (**d**) Microscope image of botryoidal dolomite (Sample HF-Dn1) from the 2nd Member in the Hanfengya profile merged by 13 views, showing petrological appearance of the host rock (MD) and vugs filled with five stages of dolomite cement defined in this study; (**e**) the emerged CL images of (**d**), yellow arrows indicate the rim structure; (**f**) Outcrop image from the 4th Member in the Bajiaoxi profile showing the intraclastic bindstone to grainstone; (**g**) Thin section image from the 4th Formation in the Bajiaoxi profile (Sample BJ-Dn4), which consists of intraclastic bindstone to grainstone, displaying various types of intraclasts (IN), cements, and interparticle pores (blue impragnate); (**h**) the CL image of (**g**).

By contrast, the intraclastic bindstone to grainstone are relatively homogeneous (Figure 4f). The microscopic image clearly exhibits the intraclasts (IN) made up of microbial-related fabrics and micritic dolomite and interparticle pores (Figure 4g). The pores are

completely or partially filled with dolomite cements. CL microscopy reveals that the host rock displays dull luminescence, whereas the rims of crystalline dolomite cements display bright luminescence (Figure 4h).

4.2. Results for Geochronology and Geochemistry

Geochronology and geochemistry results are listed in Table 1, and shown in Figures 5 and 6.

Table 1. Summary of geochemical data of the microbialite from the Dengying Formation, Eastern Sichuan and Central Sichuan.

Regions	Fabrics	Formation/ Profile	Sample No.	U-Pb Dating(Ma)	C & O Isotope Ratio/‰(VPDB)		$^{87}Sr/^{86}Sr$		CL Color Observed
					$\delta^{13}C$	$\delta^{18}O$	Values	Mean	
Eastern Sichuan	host rock of thrombolite	Z_2dn2/Hanfengya profile	HF-Z_2dn2-1	580 ± 9.8	3.45	−4.525	0.70960, 0.70934, 0.70909, 0.70947, 0.7092, 0.70943, 0.70932	0.709350	Dull-dark orange
	Fibrous dolomite cement	Z_2dn2/Hanfengya profile	HF-Z_2dn2-1	579 ± 11	3.115	−3.668	0.70941, 0.70932, 0.7095, 0.70932, 0.70958	0.709426	Dark orange
	Bladed dolomite cement	Z_2dn2/Hanfengya profile	HF-Z_2dn2-1	479 ± 10	3.619	−6.046	0.7082, 0.70866, 0.70898, 0.70865	0.708623	Dark orange
	Brown-dark dolomite cement	Z_2dn2/Hanfengya profile	HF-Z_2dn2-1				0.7093, 0.70928, 0.70920, 0.70973	0.709378	Dull
				$450 \pm 11,$ 449 ± 13	2.38	−6.618	0.70811, 0.70865, 0.70898, 0.70872, 0.70876	0.708644	Dark orange-orange red
	Fine crystalline dolomite cement	Z_2dn2/Hanfengya profile	HF-Z_2dn2-1	/	3.484	−5.453	0.70782, 0.7087, 0.70821, 0.7087, 0.70904	0.708494	Medium orange red
	Medium-coarse crystalline dolomite cement	Z_2dn2/Hanfengya profile	HF-Z_2dn2-1	373 ± 79	2.681	−6.93	0.70892, 0.70954, 0.7097, 0.70974	0.709475	Bright orange red
	Fibrous dolomite cement	Z_2dn4/Bajiaoxi profile	BJ-Z_2dn4-4	521 ± 21	2.644	−4.452	0.7092		Dull
Central Sichuan	host rock	Z_2dn2/Xianfeng profile	XF-Z2dn2-S4	584 ± 32	1–3	−4 to −1	0.708718		Non-luminescent
	Isopachous dolomite cement	Z_2dn2/Xianfeng profile	XF-Z2dn2-S5	546 ± 7.6	1–3	−6 to −4	0.708732		Non-luminescent
	Rayed dolomite cement	Z_2dn2/Xianfeng profile	XF-Z2dn2-S4	516 ± 10	2–4	−8 to −6	0.709351		Dark orange dim
	Bladed dolomite cement	Z_2dn2/Well Moxi-22	MX22-Z2d2-2	499 ± 25	0–2	−8 to −4	/		Dim

Geochemistry data from the Central Sichuan after [24].
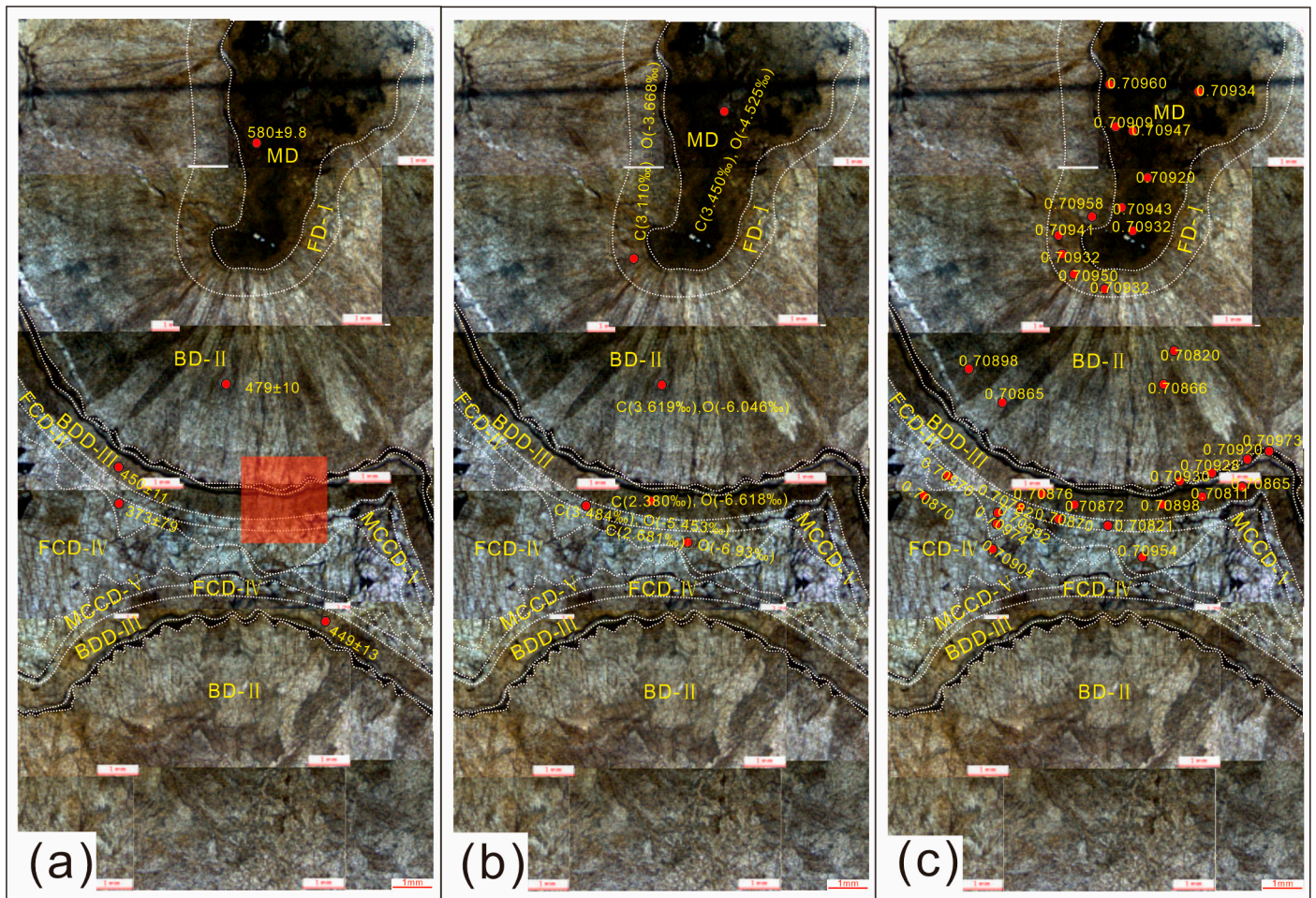
Figure 5. Photographs showing the results of in situ laser ablation U-Pb dating (**a**), carbon and oxygen isotopes (**b**), and $^{87}Sr/^{86}Sr$ (**c**) on the different fabric of Botryoidal dolomite. Please note that the red square in (**a**) highlights the area for which elemental mapping area was completed.

4.2.1. Laser Ablation U-Pb Dating

Seven U-Pb geochronology ages were obtained from host rocks and four fabrics of dolomite cements (Figures 5 and 6). The host rock of the 2nd Member of the Dengying Formation yields a U-Pb age of 580 ± 9.8 Ma (Table 1 and Figures 5a and 6a); the FD-I cement, BD-II cement, BDD-III cements, and MCCD-V cement from the 2nd Member of the Dengying Formation yields U-Pb ages of 579 ± 11 Ma (Figures 5a and 6b), 479 ± 10 Ma (Figures 5a and 6c), 450 ± 11 Ma and 449 ± 13 Ma (Figures 5a and 6d,e), and 373 ± 79 Ma (Figures 5a and 6f), respectively. Additionally, the fibrous dolomite cement from the 4th Member of the Dengying Formation yields a U-Pb age of 521 ± 21 Ma (Figure 6g).

4.2.2. Laser Ablation Carbon and Oxygen Isotopes

The $\delta^{13}C$ and $\delta^{18}O$ values of the Dengying Formation from this study both vary greatly for the different phases of dolomite cements in the study area. The host rocks from the 2nd Member and 4th Member yield $\delta^{13}C$ values average at 3.45‰ and 2.736‰ (VPDB), respectively, and the $\delta^{18}O$ values average at -4.525‰ and -3.935‰ (VPDB), respectively. Fibrous dolomite cement from the 2nd Member and 4th Member has average $\delta^{13}C$ value of 3.115‰ and 2.644‰ (VPDB), respectively, and the $\delta^{18}O$ values are between -3.668‰ and -4.452‰ (VPDB), respectively (Figure 5b). The BD-II cement from the 2nd Member yields an average $\delta^{13}C$ and $\delta^{18}O$ value of 3.619‰ (VPDB) of -6.046‰ (VPDB) (Figure 5b). The BDD-III cements yield slightly depleted $\delta^{13}C$ and $\delta^{18}O$ values average at 2.38‰ (VPDB) and at -6.618‰ (VPDB), respectively (Figure 5b). The FCD-IV cements yield relatively positive

average δ^{13}C and δ^{18}O value of 3.484‰ (VPDB) and −5.453‰ (VPDB), respectively. The MCCD-V cements display relative low average δ^{13}C and δ^{18}O value of 2.681‰ (VPDB) and −6.93‰ (VPDB), respectively.
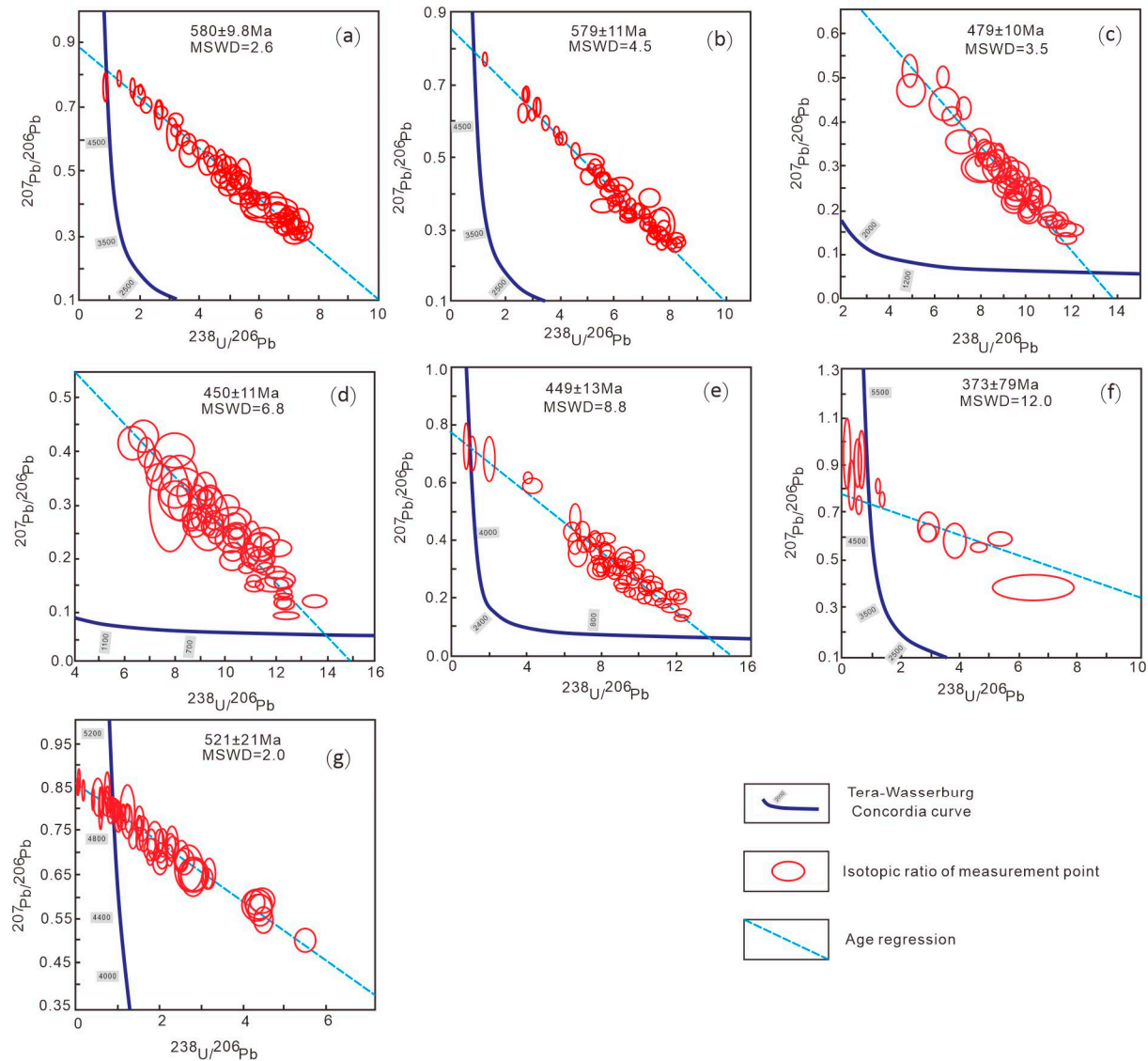
Figure 6. The U-Pb dating results from different fabrics of the microbial dolomite in the Dengying Formation, Eastern Sichuan (the sample ages were regressed on Tera-Wasserburg plots using Isoplot 3.0 [55] after raw data were processed by Iolite 3.6 [56]). (**a**) The host rock of the thrombolite dolostone (MD), formed at 580 ± 9.8 Ma, sample HF-Dn2, the 2th Member of the Dengying Formation in the Hanfengya profile; (**b**) the fibrous dolomite (FD-I), formed at 579 ± 11 Ma, sample HF-Dn2, the 2th Member of the Dengying Formation in the Hanfengya profile; (**c**) the Bladed dolomite (BD-II), formed at 479 ± 10 Ma, sample HF-Dn1, the 2nd Member of the Dengying Formation in the Hanfengya profile; (**d**) the brown-dark dolomite cement (BDD-III), formed at 450 ± 11 Ma, sample HF-Dn1, the 2nd Member of the Dengying Formation in the Hanfengya profile; (**e**) the brown-dark dolomite cement (BDD-III), formed at 449 ± 13 Ma, sample HF-Dn1, the 2nd Member of the Dengying Formation in the Hanfengya profile; (**f**) the medium-coarse crystalline dolomite (MCCD-IV), formed at 373 ± 79 Ma, sample HF-Dn1, the 2nd Member of the Dengying Formation in the Hanfengya profile; (**g**) The fibrous dolomite (FD-I), formed at 521 ± 21 Ma, sample BJ-Dn4, the 4th Member of the Dengying Formation in the Bajiaoxi profile.

4.2.3. Laser Ablation Strontium Isotope Ratios

Thirty-five ^{87}Sr/^{86}Sr ratios of microbial dolomites from the 2nd and 4th Members of Dengying Formation were measured. The ^{87}Sr/^{86}Sr ratios of the host rocks from the 2nd Members of Dengying Formation ranges from 0.70909 to 0.70960 (Figure 5c; Table 1), with an average at 0.70935 (n = 7), being consistent with the coeval seawater range (0.7086–0.7096; [57]). The ^{87}Sr/^{86}Sr ratios of the FD-I cements lies between 0.70932 and 0.70958 (Figure 5c; Table 1), average at 0.709426 (n = 5), which is slightly higher than that of the host rock. Both BD-II and BDD-III cements show markedly low ^{87}Sr/^{86}Sr ratios ranging from 0.70820 and 0.70898 (Table 1), averaging at 0.708623 (n = 4), and from 0.70811 to 0.70898 (Table 1), with an average at 0.708644 (n = 5), respectively. However, a thin layer between these two types of dolomite cements has markedly high strontium isotope ratios of 0.70920–0.70973, with an average at 0.709378 (n = 4) (Figure 5c; Table 1). The FCD-IV dolomite cements display the lowest ^{87}Sr/^{86}Sr ratios ranging from 0.70782 to 0.70904 (Table 1), with an average at 0.708494 (n = 5). The MCCD-V dolomites have markedly elevated ^{87}Sr/^{86}Sr ratios lying between 0.70892 and 0.70974, averaging at 0.709475 (n = 4) (Table 1). The strontium isotope ratios of the fibrous dolomite (0.7092, n = 1) from the 4th Members of Dengying Formation is similar to the ones from the 2nd Members.

4.2.4. Elemental Mapping of Trace Elements and Rare Earth Elements

Based on the microscopic and cathodoluminescence observations (Figure 7a,b), this research subsequently performed an elemental mapping analysis of trace elements and REEs as well as Mg and Ca for BD-II, BDD-III, FCD-IV, and MCCD-V cements within sample HF-Dn1. These data shows that the different fabrics display similar Mg and Ca contents but variable U, Mn, Fe, Sr, Ce, and Eu contents (Figure 7).

The BD-II cements generally have lower U, Mn, Fe, and Ce contents, which is marked with blue-brown bands (Figure 7e–g,i), although the presence of few small red-yellow spots represent areas of high concentration values. The BDD-III cements mostly yield relatively high Sr values (red band; Figure 7h) and low U, Mn, Fe, and Ce values (blue bands; Figure 7e–g,i), with some thin laminations marked with high U, Mn, Fe, and Ce values. It is also consistent with the CL microscopy observations which showing the dark orange-orange red luminescence (Figure 7b) with some thin laminated orange luminescence. The FCD-IV cement exhibits high Mn and Fe values (red-yellow bands; Figure 7f,g) but low U, Sr, Ce, and Eu values (blue band; Figure 7e,h–j), with dark red luminescence under CL excitation (Figure 7b). The MCCD-V exhibits low U, Mn, Fe, and Ce values (blue bands; Figure 7f,g,i) but high Sr values (red band; Figure 7h), and displays bright orange red luminescence under CL (Figure 7b). All these dolomites broadly have relatively low Eu and Th values (blue-brown bands; Figure 7j,k), excepting the boundaries between BD-II and BDD-III cements, which showing high Eu and Th values along with high U, Mn, Fe, Sr, and Ce values.
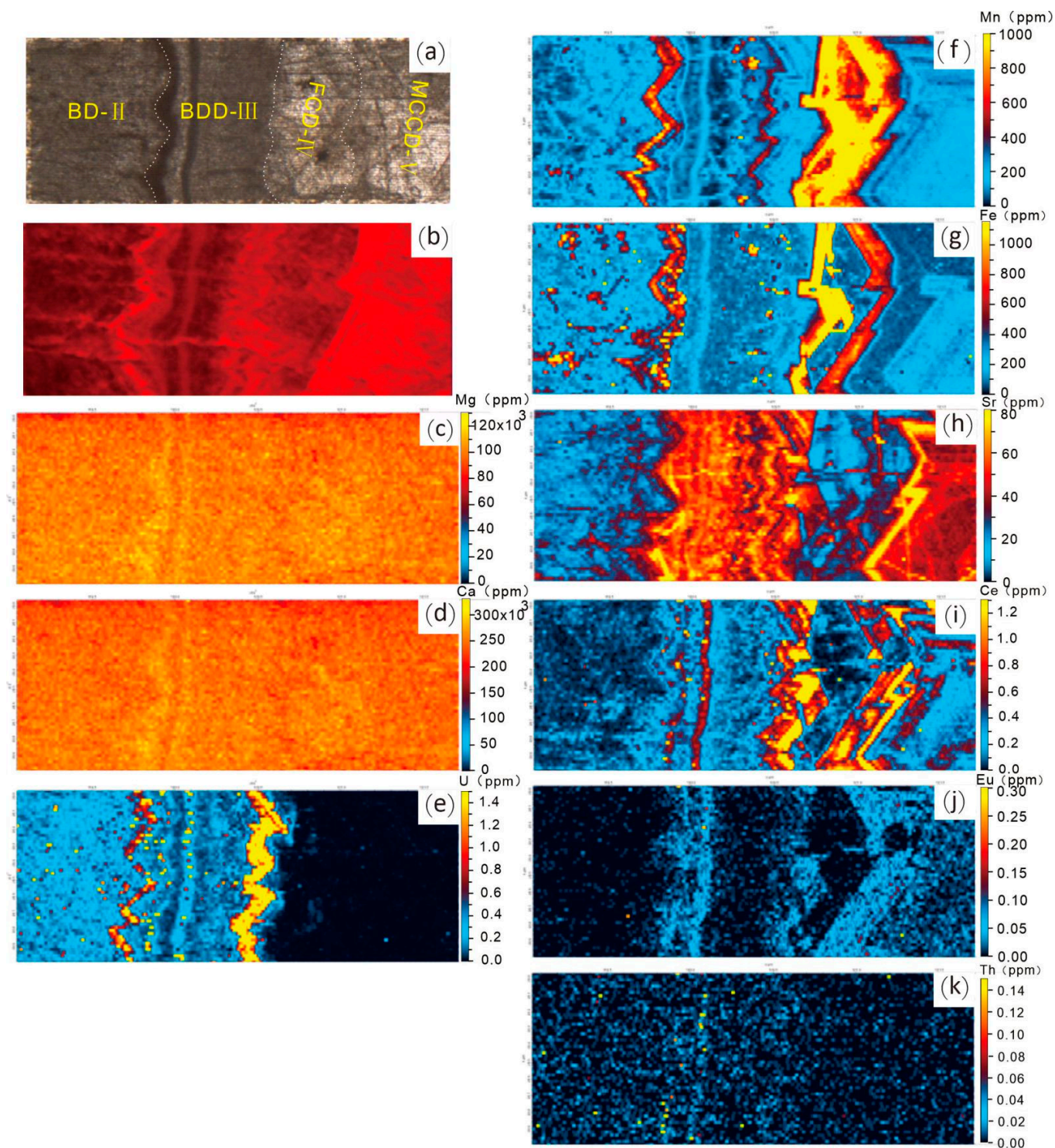
Figure 7. Elemental mapping of the botryoidal structure of sample HF-Dn1-1; (**a**) thin section image; (**b**) the CL image; (**c**) planar distribution of the Mg content; (**d**) planar distribution of the Ca content; (**e**) planar distribution of the U content; (**f**) planar distribution of the Mn content; (**g**) planar distribution of the Fe content; (**h**) planar distribution of the Sr content; (**i**) planar distribution of the Ce content; (**j**) planar distribution of the Eu content; (**k**) planar distribution of the Th content. The location of the mapping area is shown in Figure 5a.

5. Discussion

5.1. Evaluation of Diagenetic Modification

Theoretically, U-Pb dating requires a closed system after mineral precipitation [58], because its geochemistry may be modified by extraneous fluid alterations in open systems. Since the Dengying Formation has experienced long and complex diagenetic alterations, i.e., burial and exposure, it is thus necessary to evaluate their effects on the U-Pb ages before any interpretation is made.

Mazzullo [59] proposed several criteria for identifying diagenetic dolomites as burial depth increases, which include the transformation of initial dolomite with small crystals to: (1) more stoichiometric and higher ordered phases; (2) coarse crystalline mosaics; (3) depleted in ^{18}O and Sr and Na concentrations; and (4) homogenized cathodoluminescent color under CL. Petrographic and geochemistry characterizations suggest that all types of dolomites in the Dengying Formation, including host rock and FD-I, BD-II, and BDD-III cements, may have experienced negligible modifications according to their very fine crystals and well-preserved original rock fabric, and cathodoluminescent zonation under CL [60]. In addition, the strontium isotope compositions are comparable with the contemporaneous seawater, further support against any obvious recrystallization [54]. Therefore, the microbial dolomites of Dengying Formation in the study area are likely to have preserved primary geochronological and geochemical characteristic.

The high and variable Sr isotopes measured in our study are very similar to Sr isotope values (from 0.7089 to 0.7102, mean 0.709242, n = 48) reported by [61], obtained from the Ediacaran Dengying Formation of well PT1 from Sichuan Basin. The Sr isotopes from the Ediacaran Dengying carbonates from our study and from [61], however, were much higher than that those of generally accepted global Sr isotopic signatures of Ediacaran seawater of 0.7085–0.7090 (e.g., [61–64]). Zhang [61] attributed the high ^{87}Sr/^{86}Sr values to "the intense continental weathering with "the increased supply of terrigenous strontium" to the Sichuan Basin during the Ediacaran. In addition, the Sichuan Basin might be restricted during the latest Ediacaran [61], which led to high and variable Sr isotopes as a local phenomenon in the Ediacaran Dengying Formation in the Sichuan Basin as suggested by [61]. The other scenario for the high and variable Sr isotopes from the Ediacaran Dengying Formation from the Sichuan Basin could be related to the influences of the later diagenetic fluids that migrated up from the crystalline basement via faulty systems (e.g., [65,66]), which precipitated later digenetic carbonates and altered and reset the geochemical signatures of the precursor carbonates of the Ediacaran Dengying Formation. In this scenario, the lower Sr isotopic values could represent less altered that are closer to the original signatures. This later scenario is explored in the following discussions where it is necessary.

5.2. Determining the Diagenetic Processes and Environments

Since the host rocks have not been strongly modified by recrystallization and record primary information relating to their geochemistry, analysis of these may provide reliable U-Pb dating ages, while the carbon, oxygen, and strontium isotope values largely record their primary isotopic compositions. Additionally, the laser ablation U-Pb ages of diagenetic phases provide a solid basis for determining the absolute age of timing for their generation under the burial evolution framework, and coupled with isotope and element data, allows the various diagenetic environments to be more precisely constrained.

5.2.1. Matrix Dolomitization

The determined U-Pb age data of thrombolite dolostone from the 2nd Member of Dengying Formation is 580 $\pm$ 9.8 Ma, which is comparable with the age of the Ediacaran and one determined age of 584 $\pm$ 32 Ma obtained from its counterpart from Central Sichuan Basin (Figure 8). Taking into account their petrographic features, such as very fine-crystalline micritic dolomite and preservation of microbial fabrics (e.g., stromatolitic and thrombolytic dolomite), we interpret that U-Pb ages of matrix dolomites likely reflect the timing for matrix dolomitization [67]. Microbial dolomitization [68–70] or reflux dolomi-

tization [71] was proposed to interpret the origin of this early dolomitization event. Fluid inclusion data from the Ediacaran halite in the Yangtze area indicate that the maximum seawater temperature was approximately 39.4 ± 1.0 °C [72], corresponding to the tropical intra-atmospheric convergence zone in which the South China was located during the terminal Ediacaran Period [73]. Additionally, the measured strontium isotope ratio suggests that the dolomitizing waters were mainly derived from Ediacaran seawater [69,74].
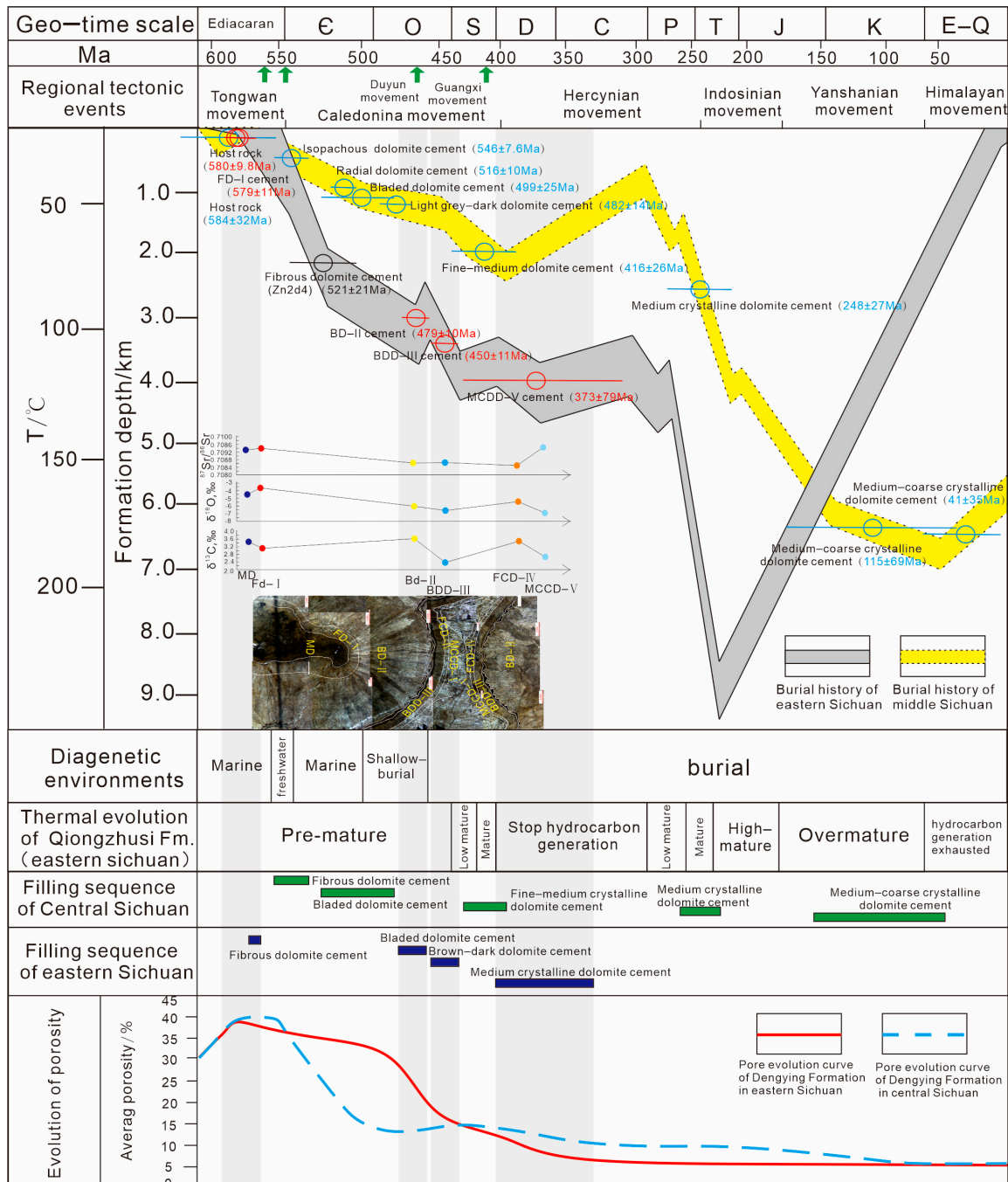
Figure 8. Burial history of the Ediacaran Dengying Formation, Sichuan Basin (the burial history of Eastern Sichuan is modified from [44]; that of Central Sichuan is modified from [45]; the porosity curve of Central Sichuan refers to [24]).

5.2.2. The Origin of Botryoidal Dolomite

The botryoidal dolomite occurs as the main filling in the vug including at least three stages of fabrics, e.g., FD-I, BD-II, and BDD-III cements. The FD-I cement in the thrombolite dolostone is dated at 579 ± 11 Ma, which is slightly younger than the host rock age data, but also falling within the Ediacaran Period, suggesting it was either a syn-depositional or very early diagenetic phase [71]. The petrographic features show that the FD-I cements are mostly framework pore-fillings with well-preserved concentric and isopachous crusting laminae, implying they were the products of direct spontaneous nucleation and in situ stabilization from the fluids under depositional environments [54,68]. The slightly elevated $^{87}Sr/^{86}Sr$ ratios (0.70932–0.70958) and depleted $\delta^{13}C$ (3.115‰) of the FD-I cements, as compared to their host rocks (Figure 8), suggesting that they were likely influenced by meteoric water. This interpretation is further supported by its platform margin facies where exposures were common, and the presence of a regional disconformity boundary above the 2nd Member of Dengying Formation, which imply a region karstification event.

The BD-II and BDD-III cements, as the main parts of botryoidal dolomite, yield U-Pb dating ages of 479 ± 10 Ma and 449 ± 13 Ma, respectively, corresponding to the Early–Middle Ordovician and Late Ordovician. These results argue against botryoidal dolomite being syn-sedimentary diagenetic products [54]. Instead, a more reasonable interpretation is that they were likely influenced by the Duyun tectonic movement, which resulted in a large-scale uplift and the denudation of the Ordovician, and an unconformity between the Ordovician and Silurian [44]. Compared with the host rock and FD-I cements, the negative $\delta^{18}O$ value of BD-II dolomite is likely related to higher crystallization temperature which is consistent with deeper burial environments (at a depth of about 3 km) (Figure 8). By adopting the calculation formulas proposed by [75,76], based on the oxygen isotope of dolomite and burial temperature of 96 °C in burial history (Figure 8), the oxygen isotope of the fluid from which the dolomite precipitated was calculated as 2.35‰ (SMOW), which is consistent with the above interpretation. Although their $^{87}Sr/^{86}Sr$ ratios is slightly lower than their host rocks and FD-I cements, this still falls within the range of Ediacaran seawater [54], suggesting a seawater-dominated dolomitizing fluid, consistent with their low U, Mn, Fe, and Ce contents (Figure 7e–g,i). We interpret that the BD-II dolomite was precipitated from the younger seawater-derived fluids during the uplifting and denudation of the Duyun movement. In contrast, BDD-III cements have more negative $\delta^{13}C$ and $\delta^{18}O$ values (2.38‰ and –6.618‰, respectively), indicating a higher crystallization temperature due to a greater burial depth (Figure 8). However, BDD-III cements show $^{87}Sr/^{86}Sr$ ratio of 0.70811–0.70898, low U, Mn, Fe, Ce, and Eu contents, compared with to those of the BD-II cements, suggesting they may have precipitated under similar diagenetic conditions [54,77–79]. Please note that a thin layer between the BD-II cement and BDD-III cement displays higher contents of U, Mn, Fe, Ce, Sr, and Th (Figure 7) and $^{87}Sr/^{86}Sr$ ratios (0.70920–0.70973, Figure 5c), and more negative $\delta^{13}C$ value, as compared with the BD-II cements, and may imply a temporarily exogenous fluid which was probably related to the Duyun movement with the involvement of continent-derived materials.

5.2.3. Filling of Crystalline Dolomite Cements

The MCCD-V dolomite cement is dated a 373 ± 79 Ma, spanning the Silurian and Devonian. In comparison, the FCD-IV cement has higher $\delta^{13}C$ and $\delta^{18}O$ values with lower $^{87}Sr/^{86}Sr$ ratio while the MCCD-V cement has lower $\delta^{13}C$ and $\delta^{18}O$ values with higher $^{87}Sr/^{86}Sr$ ratio (Figure 8), probably representing two stages of exogenous fluids. It is worth noting that great variations of the Mn, Fe, and Sr content between FCD-IV and MCCD-V dolomite cement (Figure 8) are observed. The FCD-IV dolomites yield high Fe^{2+} and Mn^{2+} contents (Figure 7f–h), referring to their $\delta^{13}C$ and $\delta^{18}O$ values, suggesting that they were generated during shallow burial [78]. By contrast, the MCCD-V cements show lower $\delta^{13}C$ and $\delta^{18}O$ values, indicating they may be related to exogenous fluids during deeper burial conditions. Therefore, the large error of dating result was likely caused by the alterations caused by external fluids related to regional tectonic movement during the Early

Silurian [79]. The FCD-IV and MCCD-V dolomites exhibit bright orange luminescence under CL, reflecting their deep burial conditions. The low Eu contents in these dolomites implying the lack of hydrothermal fluid interaction [80,81].

To sum up, the petrographic and geochemistry results show that the microbial dolomite in Eastern Sichuan successively experienced: (1) the Ediacaran sedimentary environment, with the constrained age of 580 ± 9.8 Ma; (2) a seawater-dominated diagenetic environment, with a constrained age of 579 ± 11 Ma (during or slightly post-dating deposition) and fluids of Ediacaran seawater; (3) a shallow-burial diagenetic environment related to the denudation during the Duyun movement, with a constrained age of 479 ± 10 Ma and involving Ediacaran seawater-derived fluids; (4) a burial diagenetic environment, with a constrained ages of 450 ± 11a and 373 ± 79 Ma and fluids of mainly seawater. The sequence helps to decipher the vuggy porosity destruction history during progressive burial since deposition or a penecontemporaneous stage.

5.3. Comparison of the Diagenesis and Reservoir-Forming Process between Eastern Sichuan and Central Sichuan

We herein have compared the similarities and differences of diagenetic and reservoir-forming model of microbial dolostone reservoirs between the Eastern and Central Sichuan Basin. Similarities include: (i) much the same microbial rock types, i.e., stomatolite dolostone, thombolite dolostone, laminated dolostone, and intraclastic bindstone [10,24]; (ii) presence of dissolved vugs with the same filling sequence of cements, i.e., the botryoidal dolomites; and (iii) nearly identical diagenetic sequences. By contrast, their differences include: (i) the U-Pb age of FD-I cement in Eastern Sichuan is older than those in Central Sichuan; (ii) the U-Pb age of BD-II and BDD-III cements in Eastern Sichuan are younger than those in Central Sichuan; (iii) the maximum depth of Central Sichuan is shallower than that of Eastern Sichuan, implying a greater influence by the tectonic uplifting movement; and (iv) the crystal sizes of MCCD-V cements in the Eastern Sichuan are smaller than that in Central Sichuan. Hence, the Dengying Formation in Central Sichuan is more readily subjected to hydrothermal fluids modification by later stage tectonic movements.

5.4. Porosity Evolution and Guidance on Exploration

Based on the porosity evolution in Central Sichuan Basin, according to the point counting evaluation of each phase of cementation, it is estimated that the initial porosity generally reached a value of 30%, which is consistent with the microbial dolomite presented by [82]. Dissolution contributed a ~10% increase in porosity during the Tongwan movement at the end of 2nd Member of Dengying Formation, so that the total porosity before prior to burial may have reached 40%. Subsequently, the FD-I cements occupied part of the reservoir space and the porosity decreased to 32% on average. The Middle Ordovician BD-II cement occupied most of the reservoir space and the average porosity rapidly dropped to 15%, while the BDD-III cements of Late Ordovician reduced the porosity to 9% on average. From Silurian to Devonian, residual pores were filled with crystalline dolomite and the average porosity declined to 6%, which was preserved afterward (Figure 8).

Based on the restored porosity evolution and burial history of the Dengying Formation in Eastern Sichuan, the effective pores before oil and gas migration were evaluated. The source rock in the study area is the Cambrian Qiongzhusi Formation developed within the Chengkou-Exi trough [83] (Figure 1c). The vugs formed before burial, mainly due to (pene-) contemporaneous dissolution (fabric-selective pores) and supergene karstification (non-fabric selective pores), with the porosity of up to 40%. The porosity reduction occurred mostly after burial, related to multi-stage cementation. The 1st to 3rd cementation stages all occur in the early Caledonian movement and predominantly affect residual vugs, with the porosity at that time of about 9%. With continued burial, the source rocks of the Qiongzhusi Formation began to mature gradually during the Silurian and started the initial oil generation in Late Silurian, immediately followed by the initial hydrocarbon migration. At that time, the porosity remained at about 11%. In response to the late Caledonian

movement during the Silurian, the study area was uplifted and hydrocarbon generation in the source rocks was suspended during Devonian-Carboniferous. With a return to more deep burial in the Permian, the source rocks of the Qiongzhusi Formation were subjected to sustained burial and a 2nd oil generation episode began, with peaks at the end of the Permian, which lead to a 2nd hydrocarbon migration into the Dengying Formation. At this time, the porosity was about 6%. From Middle Triassic to Middle Jurassic times, with an increasing burial depth, the crude oil of paleo-reservoirs cracked and produced gas, according to the result from Central Sichuan Basin [84]. Thus, the reservoir of the Dengying Formation in the study area presents good storage capacity upon arrival of the two oil generation peaks and thus has high hydrocarbon accumulation potential.

Although there are differences in the diagenetic process between the Eastern and Central Sichuan Basins, the key to studies on the reservoir is the hydrocarbon accumulation process—whether or not effective pores are formed prior to oil and gas migration. The dolomite reservoirs of Dengying Formation in Central Sichuan and Eastern Sichuan are highly similar, in terms of petrology, reservoir space type, and diagenetic sequence. The burial history shows that the cementation (mineral filling) of the Dengying Formation in both Central Sichuan and Eastern Sichuan occurred during the early Caledonian movement, by which time the porosity decreased to 15% in Central Sichuan and to 9% in Eastern Sichuan, prior to oil and gas accumulation. The hydrocarbons of microbialite in Central and Eastern Sichuan are sourced from the Cambrian Qiongzhusi Formation [85]. Specifically, at the two hydrocarbon generation peaks, the porosities in Central Sichuan and Eastern Sichuan were estimated at ~12% to 15% and from 6% to 11%, respectively, implying high reservoir quality. The petroleum system in Central Sichuan is concentrated in the Gaoshiti-Moxi area on both sides of the Deyang-Anyue rift of the western margin of the Leshan-Longnüsi paleo-uplift, where the Weiyuan gas field and the Anyue gas field have been successively discovered. Similarly, the petroleum system in Eastern Sichuan is also located at a paleo-geomorphic highland, i.e., the Xuanhan-Kaijiang paleo-uplift area [86]. Therefore, we anticipate that the platform margins on both sides of the Chengkou-Exi rift of the eastern margin of the Xuanhan-Kaijiang paleo-uplift are favorable exploration targets.

6. Conclusions

This research considered key field profiles and rock fabric characteristics in an effort to decipher the formation and evolution histories of microbial dolomite from the Eastern Sichuan Basin. By application of new technologies applied to diagenesis, such as elemental mapping, laser ablation U-Pb dating, and also tests such as laser ablation in situ isotope analyses of carbon, oxygen, and strontium, we successfully concluded that the Ediacaran microbial dolomite in Eastern Sichuan progressively experienced synsedimentary dolomitization, penecontemporaneous cementation of FD-I cement, Ordovician cementation of BD-II and BDD-III cements, and Silurian-Devonian fillings of MCD-IV and MCCD-V cements. Dolomite fillings at each stage are mainly derived from seawater-derived fluids with temporarily exogenous fluid involvement. Furthermore, due to differential effects of tectonic movement, the mineral filling of Eastern Sichuan is delayed and thus its pore evolution is differentiated from that of the Central Sichuan. As such, our analysis of the diagenesis-reservoir-forming process clarifies that the Dengying Formation in the study area maintained a high porosity of 6%–11% during the two oil generation peaks of the Qiongzhusi Formation and therefore has high potential for hydrocarbon accumulation. The platform margin at the eastern edge of the Xuanhan-Kaijiang paleo-uplift is demarcated as the next key exploration target in this part of China.

References

1. Bosence, D.; Gibbons, K.; Le Heron, D.P.; Morgan, W.A.; Pritchard, T.; Vining, B.A. Microbial carbonates in space and time: Introduction. *Geol. Soc.* **2015**, *418*, 1–15. [CrossRef]
2. Mancini, E.A.; Benson, D.J.; Hart, B.S.; Balch, R.S. Reef reservoirs associated with paleotopographic basement structures. *AAPG Bull.* **2000**, *84*, 1699–1717.
3. Mancini, E.A.; Llinas, J.C.; Parcell, W.C.; Aurell, M.; Badenas, B.; Leinfelder, R.R.; Benson, D.J. Upper Jurassic thrombolite reservoir play, northeastern Gulf of Mexico. *AAPG Bull.* **2004**, *88*, 1573–1602. [CrossRef]
4. Wright, P.V.; Racey, A. Pre-salt microbial carbonate reservoirs of the Santos Basin, offshore Brazil. In Proceedings of the AAPG Annual Convention and Exhibition, Denver, CO, USA, 7–10 June 2009; pp. 7–10.
5. Grotzinger, J.P.; Amthor, J.E. Facies and reservoir architecture of isolated microbial carbonate platforms, terminal Proterozoic-early Cambrian Ara Group, South Oman Salt Basin. In Proceedings of the AAPG Annual Convention and Exhibition, Houston, TX, USA, 1–13 March 2002; pp. 10–13.
6. Schröder, S.; Grotzinger, J.P.; Amthor, J.E.; Matter, A. Carbonate deposition and hydrocarbon reservoir development at the Precambrian–Cambrian boundary: The Ara Group in South Oman. *Sediment. Geol.* **2005**, *180*, 1–28. [CrossRef]
7. Kenter, J.A.; Harris, P.M.M.; Porta, G.D.; Fischer, D.; Weber, A.J. Microbial and cement boundstone-dominated flanks (and reservoirs) of an isolated carbonate platform. In Proceedings of the AAPG Annual Convention, Dallas, TX, USA, 18–21 April 2004.
8. Wei, G.Q.; Yang, W.; Liu, M.C.; Xie, W.R.; Jin, H.; Wu, S.J.; Su, N.; Shen, J.H.; Hao, C.G. Distribution rules, main controlling factors and exploration directions of giant gas fields in the Sichuan Basin. *Nat. Gas Ind.* **2019**, *39*, 1–12. [CrossRef]
9. Li, J.Z.; Gu, Z.D.; Lu, W.H.; Jiang, H.; Zhai, X.F.; Liu, G.X.; Zhao, R.R. Main factors controlling the formation of giant marine carbonate gas fields in the Sichuan Basin and exploration ideas. *Nat. Gas Ind.* **2021**, *41*, 13–26.
10. Chen, Y.N.; Shen, A.J.; Pan, L.Y.; Zhang, J.; Wang, X.F. Features, origin and distribution of microbial dolomite reservoirs: A case study of 4th Member of Sinian Dengying Formation in Sichuan Basin, SWChina. *Pet. Explor. Dev.* **2017**, *44*, 704–715. [CrossRef]
11. Feng, M.Y.; Wu, P.C.; Qiang, Z.T.; Liu, X.H.; Duan, Y.; Xia, M.L. Hydrothermal dolomite reservoir in the Precambrian Dengying Formation of central Sichuan Basin, southwestern China. *Mar. Pet. Geol.* **2017**, *82*, 206–219. [CrossRef]
12. Hu, A.P.; Sheng, A.J.; Yang, H.X.; Zhang, J.; Wang, X.; Yang, L.; Meng, S.X. Dolomite genesis and reservoir-cap rock assemblage in carbonate-evaporite paragenesis system. *Pet. Explor. Dev.* **2019**, *46*, 916–928. [CrossRef]
13. Chen, Z.Q. Gas Exploration in Sinian Dengying Formation, Sichuan Basin. *China Pet. Explor.* **2010**, *15*, 1–14.
14. Shi, Z.J.; Liang, P.; Wang, Y.; Hu, X.Q.; Tian, Y.M.; Wang, C.C. Geochemical characteristics and genesis of grapestone in Sinian Dengying Formation in south-eastern Sichuan Basin. *Acta Petrol. Sin.* **2011**, *27*, 2263–2271.
15. Fang, S.X.; Hou, F.H.; Dong, Z.X. Non-stromatoltite ecologic system cyanobacteria dolostone in Dengying Formation of Upper-Sinian. *Acta Petrol. Sin.* **2003**, *21*, 96–105.
16. Wang, W.Z.; Yang, Y.M.; Wen, L.; Luo, B.; Luo, W.J.; Xia, M.L.; Sun, S.N. A study of sedimentary characteristics of microbial carbonate: A case study of the Sinian Dengying Formation in Gaomo area, Sichuan Basin. *Geol. China* **2016**, *43*, 306–318.
17. Song, J.M.; Liu, S.G.; Sun, W.; Wu, W.H.; Wang, G.Z.; Peng, H.L.; Tian, Y.H.; Zhong, Y. Control of Xingkai taphrogenesis on Dengying Formation high quality reservoirs in Upper Sinian of Sichuan Basin, China. *J. Chengdu Univ. Technol.* **2013**, *40*, 658–670.
18. Feng, M.Y.; Qiang, Z.T.; Shen, P.; Zhang, J.; Tao, Y.Z.; Xia, M.L. Evidence for hydrothermal dolomite of Sinian Dengying Formation in Gaoshiti-Moxi area, Sichuan Basin. *Acta Petrol. Sin.* **2016**, *37*, 587–598.
19. Su, Z.T.; She, W.; Liao, H.H.; Hu, S.L.; Liu, G.Q.; Ma, H. Research progress and development trend of the genesis of dolomite reservoirs. *Nat. Gas Geosci.* **2022**, *33*, 1175–1188. [CrossRef]
20. Ulrich, T.; Kamber, B.S.; Jugo, P.J.; Tinkham, D.K. Imaging element-distribution patterns in minerals by laser ablation—Inductively coupled plasma—Mass spectro-metry (LA-ICP-MS). *Can. Mineral.* **2009**, *47*, 1001–1012. [CrossRef]
21. Webb, G.E.; Kamber, B.S. Trace element geochemistry as a tool for interpreting microbialites. In *Earliest Life on Earth: Habitats, Environments and Methods of Detection*; Springer: Berlin/Heidelberg, Germany, 2011; pp. 127–170.
22. Hu, A.P.; Li, X.Z.; Jiang, Y.M.; Hu, Y.Y.; Zhang, J. Development and application of microarea geochemistry analysis technology for carbonate reservoirs. *Nat. Gas Geosci.* **2014**, *25*, 116–123.

23. Wang, F.Y.; Ge, C.; Ning, S.Y.; Nie, L.Q.; Zhong, G.X.; Noel, C.W. A new approach to LA-ICP-MS mapping and application in geology. *Acta Petrol. Sin.* **2017**, *33*, 3422–3436.

24. Shen, A.J.; Hu, A.P.; Chen, T.; Liang, F.; Pan, W.Q.; Feng, Y.X.; Zhao, J.X. Laser ablation in situ U-Pb dating and its application to diagenesis-porosity evolution of carbonate reservoirs. *Pet. Explor. Dev.* **2019**, *46*, 1062–1074. [CrossRef]

25. Yang, H.X.; Hu, A.P.; Zheng, J.F.; Liang, F.; Luo, X.Y.; Feng, Y.X.; Sheng, A.J. Application of mapping and dating techniques in the study of ancient carbonate reservoirs: A case study of Sinian Qigebrak Formation in northwestern Tarim Basin, NW China. *Pet. Explor. Dev.* **2020**, *47*, 935–946. [CrossRef]

26. Hu, A.P.; Shen, A.J.; Wang, Y.S.; Pan, L.Y.; Liang, F.; Luo, X.Y.; She, M.; Chen, W.; Qing, Y.J.; Wang, H. The progress and application of experimental analysis technology for marine carbonate reservoir. *Mar. Orig. Pet. Geol.* **2020**, *25*, 1–11.

27. Pan, L.Y.; Shen, A.J.; Zhao, J.X.; Hu, A.P.; Hao, Y.; Liang, F.; Feng, Y.X.; Wang, X.F.; Jiang, L. LA-ICP-MS U-Pb geochronology and clumped isotope constraints on the formation and evolution of an ancient dolomite reservoir: The Middle Permian of northwest Sichuan Basin (SW China). *Sediment. Geol.* **2020**, *407*, 105728. [CrossRef]

28. Pan, L.Y.; Hu, A.P.; Liang, F.; Jiang, L.; Hao, Y.; Feng, Y.X.; Shen, A.J.; Zhao, J.X. Diagenetic conditions and geodynamic setting of the middle Permian hydrothermal dolomites from southwest Sichuan Basin, SW China: Insights from in situ U–Pb carbonate geochronology and isotope geochemistry. *Mar. Pet. Geol.* **2021**, *129*, 105080. [CrossRef]

29. Qiao, Z.F.; Zhang, S.N.; Sheng, A.J.; Hu, A.P.; Liang, F.; Luo, X.Y.; She, M.; Lv, X.J. Laser ablated U-Pb dating-based determination of burial dolomitization process: A case study of Lower Ordovician Penglaiba Formation of Yonganba Outcrop in Tarim Basin. *Acta Petrol. Sin.* **2020**, *36*, 3493–3509.

30. Qiao, Z.F.; Shao, G.M.; Luo, X.Y.; Cao, P.; Sun, X.W.; Sheng, A.J. Genetic classification and large-scale reservoir development law of burial dolomite: Cognition based on LA-ICP-MS trace elemental mapping and U-Pb dating. *Nat. Gas Ind.* **2021**, *41*, 46–56.

31. Liu, H.; Feng, Z.H.; Shao, H.M.; Zhang, J.L.; Zhang, Z.W.; Zhang, Y.J.; Lu, X.; Zhang, G.Y. Application of U-Pb dating technique in the study of hydrothermal activities of dolomite reservoir: A case study on 3rd Member of Yingshan Formation in Gucheng area, Tarim Basin, NW China. *Acta Petrol. Sin.* **2022**, *38*, 765–776.

32. Zhou, J.G.; Yu, Z.; Wu, D.X.; Ren, J.F.; Zhang, D.F.; Wang, S.Y.; Yin, C.; Liu, Y.X. Restoration of formation processes of dolomite reservoirs based on laser U-Pb dating: A case study of Ordovician Majiagou Formation, Ordos Basin, NW China. *Pet. Explor. Dev.* **2022**, *49*, 1–11. [CrossRef]

33. Li, Q.; Parrish, R.R.; Horstwood, M.S.A.; Mcarther, J.M. U-Pb dating of cements in Mesozoic ammonites. *Chem. Geol.* **2014**, *376*, 76–83. [CrossRef]

34. Godeau, N.; Deschamps, P.; Guihou, A.; Leonide, P.; Tendil, A.; Gerdes, A.; Girard, J.P. U-Pb dating of calcite cement and diagenetic history in microporous carbonate reservoirs: Case of the Urgonian Limestone, France. *Geology* **2018**, *46*, 247–250. [CrossRef]

35. MacDonald, J.M.; Faithfull, J.W.; Roberts, N.M.W.; Davies, A.J.; Holdsworth, C.M.; Newton, M.; John, C.M. Clumped-isotope palaeothermometry and LA-ICP-MS U–Pb dating of lava-pile hydrothermal calcite veins. *Contrib. Mineral. Petrol.* **2019**, *174*, 63. [CrossRef]

36. Hagen-Peter, G.; Wang, Y.; Hints, O.; Prave, A.R.; Lepland, A. Late diagenetic evolution of Ordovician limestones in the Baltoscandian basin revealed through trace-element mapping and in situ U–Pb dating of calcite. *Chem. Geol.* **2021**, *585*, 120563. [CrossRef]

37. He, D.F.; Li, D.S.; Zhang, G.W.; Zhao, L.Z.; Fan, C.; Lu, R.Q.; Wen, Z. Formation and evolution of multi-cycle superposed Sichuan Basin, China. *Chin. J. Geol.* **2011**, *46*, 589–606.

38. Wang, Z.C.; Jiang, H.; Chen, Z.Y.; Liu, J.J.; Ma, K.; Li, W.Z.; Xie, W.R.; Jiang, Q.C.; Zhai, X.F.; Shi, S.Y.; et al. Tectonic paleogeography of Late Sinian and its significances for petroleum exploration in the middle-upper Yangtze region, South China. *Pet. Explor. Dev.* **2020**, *47*, 884–897. [CrossRef]

39. Yang, R. Pore Structure and Tracer-Containing Fluid Migration in Connected Pores of Wufeng and Longmaxi Shales from Western Hubei and Eastern Chongqing Regions. Ph.D. Thesis, China University of Geosciences, Wuhan, China, 2018.

40. Yang, Z.Y.; Sun, Z.M.; Yang, T.S.; Pei, J.L. A long connection (750–380 Ma) between South China and Australia: Paleomagnetic constraints. *Earth Planet. Sci. Lett.* **2004**, *220*, 423–434. [CrossRef]

41. Li, Y.Q.; He, D.F.; Wen, Z. Palaeogeography and tectonic-depositional environment evolution of the Late Sinian in Sichuan Basin and adjacent areas. *J. Palaeogeogr.* **2013**, *15*, 231–245.

42. Yang, Y.; Huang, X.P.; Zhang, J.; Yang, G.; Song, J.R.; Song, L.K.; Hong, H.T.; Tan, X.C.; Wen, L. Features and geologic significances of the top Sinian karst landform before the Cambrian deposition in the Sichuan Basin. *Nat. Gas Ind.* **2014**, *34*, 38–43.

43. Liu, H.; Luo, S.C.; Tan, X.C.; Li, L.; Lian, C.B.; Zeng, W.; Luo, B.; Shan, S.J. Restoration of paleokarst geomorphology of Sinian Dengying Formation in Sichuan Basin and its significance, SW China. *Pet. Explor. Dev.* **2015**, *42*, 311–322. [CrossRef]

44. Xu, Y.G. Reasons for Formation of Typical Palaeo-Reservoirs of Paleozoic in Southern China and Revelation to Exploration. Ph.D. Thesis, Chengdu University of Technology, Chengdu, China, 2010.

45. Li, L.; Wang, T.S.; Wang, Z.C.; Jiang, H.; Lu, W.H.; Huang, T.P. The Characteristics and Implications of Late Gas Accumulation in the Sinian Dengying Formation of Sichuan Basin. *Nat. Gas Ind.* **2014**, *25*, 1378–1386.

46. Riding, R. Microbial carbonates: The geological record of calcified bacterial–algal mats and biofilms. *Sedimentology* **2000**, *47*, 179–214. [CrossRef]

47. Dunham, R.J. Classification of Carbonates Rocks According to Deposicional texture. *Mem. Am. Assoc. Petrol. Geol.* **1962**, *1*, 108–121.

48. Gregg, J.M.; Sibley, D.F. Epigenetic dolomitization and the origin of xenotopic dolomite texture. *J. Sediment. Res. Sect. A* **1984**, *54*, 908–931.

49. Tucker, M.E.; Wright, V.P. *Carbonate Sedimentology*; Wiley: Oxford, UK, 1990; 482p.

50. Choquette, P.W.; Pray, L.C. Geologic nomenclature and classification of porosity in sedimentary carbonates. *AAPG Bull.* **1970**, *54*, 207–250.

51. Lønøy, A. Making sense of carbonate pore systems. *AAPG Bull.* **2006**, *90*, 1381–1405. [CrossRef]

52. Weber, M.; Lugli, F.; Hattendorf, B.; Scholz, D.; Mertz-Kraus, R.; Guinoiseau, D.; Jochum, K.P. NanoSr-A New Carbonate Microanalytical Reference Material for In Situ Strontium Isotope Analysis. *Geostand. Geoanal. Res.* **2020**, *44*, 69–83. [CrossRef]

53. Paton, C.; Woodhead, J.D.; Hellstrom, J.C.; Hergt, J.M.; Greig, A.; Maas, R. Improved laser ablation U-Pb zircon geochronology through robust downhole fractionation correction, Geochem. *Geophys. Geosyst.* **2010**, *11*, Q0AA06. [CrossRef]

54. Wang, J.; He, Z.; Zhu, D.; Liu, Q.; Ding, Q.; Li, S.; Zhang, D. Petrological and geochemical characteristics of the botryoidal dolomite of Dengying Formation in the Yangtze Craton, South China: Constraints on terminal Ediacaran "dolomite seas". *Sediment. Geol.* **2020**, *406*, 105722. [CrossRef]

55. Ludwig, K.R. *A Geochronological Toolkit for Microsoft Excel*; Berkeley Geochronology Center: Berkeley, CA, USA, 2003; pp. 1–70.

56. Paton, C.; Hellstrom, J.; Paul, B.; Woodhead, J.; Hergt, J. Iolite: Freeware for the visualisation and processing of mass spectrometric data. *J. Anal. At. Spectrom.* **2011**, *26*, 2508–2518. [CrossRef]

57. Halverson, G.P.; Dudas, F.; Maloof, A.C.; Bowring, S.A. Evolution of the $^{87}Sr/^{86}Sr$ composition of Neoproterozoic seawater. *Palaeoclimatology* **2007**, *256*, 103–129. [CrossRef]

58. Kaurova, O.K.; Ovchinnikova, G.V.; Gorokhov, I.M. U-Th-Pb systematics of Precambrian carbonate rocks: Dating of the formation and transformation of carbonate sediments. *Stratigr. Geol. Correl.* **2010**, *18*, 252–268. [CrossRef]

59. Mazzullo, S.J. Geochemical and neomorphic alteration of dolomite: A review. *Carbonates Evaporites* **1992**, *7*, 21–37. [CrossRef]

60. Hu, Y.; Cai, C.; Pederson, C.L.; Liu, D.; Jiang, L.; He, X.; Shi, S.Y.; Immenhauser, A. Dolomitization history and porosity evolution of a giant, deeply buried Ediacaran gas field (Sichuan Basin, China). *Precambrian Res.* **2020**, *338*, 105595. [CrossRef]

61. Zhang, X.; Zhou, G.; Zhang, P.; He, Y.; Wei, Z.; Wang, G.; Zhang, T.; He, W.; Ma, H.; Zhu, C.; et al. Strontium isotope and element constraints on the paleoenvironment of the latest Ediacaran in the Sichuan Basin, southeastern Tibetan Plateau. *Front. Earth Sci.* **2022**, *10*, 865709. [CrossRef]

62. Melezhik, V.A.; Pokrovsky, B.G.; Fallick, A.E.; Kuznetsov, A.B.; Bujakaite, M.I. Constraints on $^{87}Sr/^{86}Sr$ of Late Ediacaran seawater: Insight from Siberian high-Sr limestones. *J. Geol. Soc.* **2009**, *166*, 183–191. [CrossRef]

63. Li, D.; Ling, H.F.; Shields-Zhou, G.A.; Chen, X.; Cremonese, L.; Och, L.; Thirlwall, M.; Manning, C.J. Carbon and strontium isotope evolution of seawater across the Ediacaran–Cambrian transition: Evidence from the Xiaotan section, NE Yunnan, south China. *Precambrian Res.* **2013**, *225*, 128–147. [CrossRef]

64. Zhang, Y.G.; Yang, T.; Hohl, S.V.; Zhu, B.; He, T.C.; Pan, W.Q.; Chen, Y.Q.; Yao, X.Z.; Jiang, S.Y. Seawater carbon and strontium isotope variations through the late Ediacaran to late Cambrian in the Tarim Basin. *Precambrian Res.* **2020**, *345*, 105769. [CrossRef]

65. Qing, H.; Mountjoy, E.W. Formation of coarsely crystalline, hydrothermal dolomite reservoirs in the Presqu'ile barrier, Western Canada Sedimentary Basin. *AAPG Bull.* **1994**, *78*, 55–77.

66. Qing, H.; Mountjoy, E.W. Large-scale fluid flow in the Middle Devonian Presqu'ile barrier, Western Canada Sedimentary Basin. *Geol.* **1992**, *20*, 903–906.

67. Jin, M.D.; Tan, X.C.; Li, B.S.; Zhu, X.; Zeng, W.; Lian, C.B. Genesis of dolomite in the Sinian Dengying formation in the Sichuan Basin. *Acta Petrol. Sin.* **2019**, *37*, 443–454.

68. Lian, C.; Ren, G.; Qu, F.; Tan, X.; Li, L.; Zeng, W.; Hu, G.; Liu, H. Review and prospect on the botryoidal structures from the Sinian Dengying Formation, Sichuan Basin, China. *Petroleum* **2017**, *3*, 190–196. [CrossRef]

69. Hu, Y.; Cai, C.; Liu, D.; Pederson, C.L.; Jiang, L.; Shen, A.; Immenhauser, A. Formation, diagenesis and palaeoenvironmental significance of upper Ediacaran fibrous dolomite cements. *Sedimentology* **2020**, *67*, 1161–1187. [CrossRef]

70. Qian, Y.X.; Feng, J.F.; He, Z.L.; Zhang, K.Y.; Jin, T.; Dong, S.F.; Zhang, Y.D. Applications of petrography and isotope analysis of micro-drill samples to the study of genesis of grape-like dolomite of the Dengying Formation in the Sichuan Basin. *Oil Gas Geol.* **2017**, *38*, 665–676.

71. Jiang, L.; Shen, A.J.; Wang, Z.C.; Hu, A.P.; Wang, Y.S.; Luo, X.Y.; Liang, F.; Azmy, K.; Pan, L.Y. U–Pb geochronology and clumped isotope thermometry study of Neoproterozoic dolomites from China. *Sedimentology* **2022**. [CrossRef]

72. Meng, F.; Ni, P.; Schiffbauer, J.D.; Yuan, X.; Zhou, C.; Wang, Y.; Xia, M. Ediacaran seawater temperature: Evidence from inclusions of Sinian halite. *Precambrian Res.* **2011**, *184*, 63–69. [CrossRef]

73. Li, Z.X.; Evans, D.A.; Halverson, G.P. Neoproterozoic glaciations in a revised global palaeogeography from the breakup of Rodinia to the assembly of Gondwanaland. *Sediment. Geol.* **2013**, *294*, 219–232. [CrossRef]

74. Moore, C.H. *Carbonate Reservoirs: Porosity, Evolution and Diagenesis in a Sequence Stratigraphic Framework*; Elsevier: Amsterdam, The Netherlands, 2001.

75. Northrop, D.A.; Clayton, R.N. Oxygen-isotope fractionations in systems containing dolomite. *J. Geol.* **1966**, *74*, 174–196. [CrossRef]

76. Friedman, I.; O'Neil, J.R. Compilation of stable isotope fractionation factors of geochemical interest. *Geol. Surv. Prof. Pap. Am.* **1977**, *440*, 1–12.

77. Canfield, D.E.; Poulton, S.W.; Knoll, A.H.; Narbonne, G.M.; Ross, G.; Goldberg, T.; Strauss, H. Ferruginous conditions dominated later Neoproterozoic deep-water chemistry. *Science* **2008**, *321*, 949–952. [CrossRef]

78. Hood, A.S.; Wallace, M.W. Extreme ocean anoxia during the Late Cryogenian recorded in reefal carbonates of Southern Australia. *Precambrian Res.* **2015**, *261*, 96–111. [CrossRef]

79. Moffett, J.W. A Radiotracer Study of Cerium and Manganese Uptake onto Suspended Particles in Chesapeake Bay. *Geochim. Cosmochim. Acta* **1994**, *58*, 695–703. [CrossRef]

80. Shi, Z.J.; Wang, Y.; Tian, Y.M.; Wang, C.C. Cementation and diagenetic fluid of algal dolomites in the Sinian Dengying formation in Southeastern Sichuan Basin. *Sci. China Earth Sci.* **2013**, *43*, 317–328. [CrossRef]

81. Dong, Y.P.; Santosh, M. Tectonic architecture and multiple orogeny of the Qinling Orogenic Belt, Central China. *Gondwana Res.* **2016**, *29*, 1–40. [CrossRef]

82. Grotzinger, J.; Al-Rawahi, Z. Depositional facies and platform architecture of microbialite-dominated carbonate reservoirs, Ediacaran–Cambrian Ara Group, Sultanate of OmanMicrobialite Reservoirs in Oman. *AAPG Bull.* **2014**, *98*, 1453–1494. [CrossRef]

83. Guo, X.S.; Hu, D.F.; Huang, R.C.; Duan, J.B.; Jiang, Z.L.; Zhu, X. Feature of paleo-oil pools in the Sinian Dengying Formation, northeastern Sichuan Basin, and its significance to exploration. *Oil Gas Geol.* **2020**, *41*, 673–683.

84. Su, A.; Chen, H.; Feng, Y.X.; Zhao, J.X.; Wang, Z.; Hu, M.; Jiang, H.; Nguyen, A.D. In situ U-Pb dating and geochemical characterization of multi-stage dolomite cementation in the Ediacaran Dengying Formation, Central Sichuan Basin, China: Constraints on diagenetic, hydrothermal and paleo-oil filling events. *Precambrian Res.* **2022**, *368*, 106481. [CrossRef]

85. Wei, G.Q.; Wang, Z.H.; Li, J.; Yang, W.; Xie, Z.Y. Characteristics of source rocks, resource potential and exploration direction of Sinian and Cambrian in Sichuan Basin. *Nat. Gas Geosci.* **2017**, *2*, 289–302. [CrossRef]

86. Gu, Z.D.; Yin, J.F.; Jiang, H.; Li, Q.F.; Zhai, X.F.; Huang, P.H.; Peng, P.; Yang, F.; Zhang, H. Discovery of Xuanhan-kaijiang paleouplift and its significance in the Sichuan Basin, SW China. *Pet. Explor. Dev.* **2016**, *43*, 893–904. [CrossRef]